

**Optical-IR Spectral Energy Distributions of  $z > 2$  Lyman Break Galaxies**<sup>1 2</sup>

Marcin Sawicki and H. K. C. Yee

Department of Astronomy, University of Toronto, Toronto, Ontario M5S 3H8, Canada

email: sawicki@astro.utoronto.ca, hyc@astro.utoronto.ca

**ABSTRACT**

Broadband optical and IR spectral energy distributions are determined for spectroscopically confirmed  $z > 2$  Lyman break objects in the Hubble Deep Field (HDF). These photometric data are compared to spectral synthesis models which take into account the effects of metallicity and of internal reddening due to dust. It is found that, on average, Lyman break objects are shrouded in enough dust (typically  $E(B - V) \approx 0.3$ ) to suppress their UV fluxes by a factor of more than 10. The dust-corrected star formation rate in a typical HDF Lyman break object is  $\sim 60h_{100}^{-2}M_{\odot}yr^{-1}$  ( $q_0 = 0.5$ ). Furthermore, these objects are dominated by very young ( $\lesssim 0.2$  Gyr, and a median of  $\sim 25$  Myr) stellar populations, suggesting that star formation at high redshift is episodic rather than continuous. Typically, these star formation episodes produce  $\sim 10^9h_{100}^{-2}M_{\odot}$  of stars, or  $\sim \frac{1}{20}$  of the stellar mass of a present-day  $L^*$  galaxy.

**1. INTRODUCTION**

Recent observational studies of the high-redshift Universe have begun to yield direct information on the nature of the population of “normal” galaxies at  $z > 2$ . Color-selected searches have started to produce growing, spectroscopically-confirmed samples (e.g., Steidel et al. 1996a; Steidel et al. 1996b; Pascarella et al. 1996; Lowenthal et al. 1997; Steidel et al. 1997), while larger samples of objects identified solely on the basis of multicolor photometry have been used to boost statistics (e.g., Madau et al. 1996; Sawicki, Lin & Yee 1997; Connolly et al. 1997). Whether spectroscopically confirmed or not, such high- $z$  objects are often called “Lyman-break galaxies” or “U-band drop-outs”. The names reflect the fact that in these galaxies the UV flux is severely attenuated

---

<sup>1</sup>Based on observations made with the NASA/ESA *Hubble Space Telescope* obtained at the Space Telescope Science Institute, which is operated by the Association of Universities for Research in Astronomy, Inc., under NASA contract NAS 5-26555.

<sup>2</sup>Based on observations made at the Kitt Peak National Observatory, National Optical Astronomy Observatories, which is operated by the Association of Universities for Research in Astronomy, Inc. (AURA) under cooperative agreement with the National Science Foundation.

by the combined effects of internal and intergalactic Lyman line and continuum opacity. Unlike serendipitously discovered single objects, these new samples of high- $z$  galaxies are large enough to allow the study of global properties of the  $z > 2$  galaxy *population*, such as their number density, luminosity density, luminosity function, and rates of star formation and metal ejection.

Despite this recent progress, there is much that still remains unclear. Based on number densities, star formation rates, physical sizes, morphologies and masses inferred from spectral line widths, Steidel et al. (1996a) and Giavalisco, Steidel, & Macchetto (1996) argue that Lyman break objects are the spheroidal components of present-day luminous galaxies, seen in the act of formation. Using diagnostics similar to those employed by Steidel et al. and Giavalisco et al., Lowenthal et al. (1997) favor the interpretation that Lyman break objects are either progenitors of present-day low-mass spheroidal galaxies or are starbursting building blocks of more massive galaxies of today (see also Colley et al. 1997).

Estimates of star formation rates in Lyman break galaxies are based on their rest-frame UV fluxes (e.g., Steidel et al. 1996a; Madau et al. 1996; Lowenthal et al. 1997). However, even moderate amounts of dust may significantly suppress the UV flux and, hence, the inferred star formation rate. Meurer et al. (1997) have studied the UV spectral indices of HDF Lyman break galaxies and have deduced that, if ages of their stellar populations are  $\lesssim 0.3$  Gyr, reddening due to dust suppresses the UV flux fairly strongly (on average, a factor of 15 at 1600 Å). Using the same spectral indices, but assuming older ages (1 Gyr), Calzetti (1997) found the attenuation a factor of 3 lower than that arrived at by Meurer et al. (1997). These two different results, obtained from the same data, reflect the fact that both dust and aging have similar effects on the UV shape of the SED and that one can mimick the effects of the other. This dust-age degeneracy can be lifted by the addition of IR (i.e., rest-optical) data, which are sensitive to age but much less so to dust.

Ages of star-forming objects at  $z > 2$  are not well known. Steidel et al. (1996a) feel that ages younger than a few  $\times 10^7$  yr are unlikely, arguing that such young ages would imply that a large number of galaxies have to be bursting simultaneously. However, apart from the gravitationally lensed  $z = 2.72$  OB star absorption-line galaxy cB58 (Yee et al. 1996), for which fits to broadband optical and IR colors give the age of the dominant stellar population to be  $\lesssim 35$  Myr (Ellingson et al. 1996), no quantitative age measurements exist for Lyman break galaxies. Constraints on ages will lift the dust-age degeneracy, in addition to providing clues to the evolutionary history of Lyman break objects.

The Hubble Deep Field (HDF; Williams et al. 1996) is a small but intensely studied area of the sky, for which both extremely deep multiwavelength imaging (e.g., Williams et al. 1996; Dickinson et al. 1997; Hogg et al. 1997; Serjeant et al. 1997; Fomalont et al. 1997) and follow-up spectroscopy (e.g., Steidel et al. 1996b; Cohen et al. 1996; Lowenthal et al. 1997; Zepf et al. 1997) have been carried out. To date, 17 spectroscopically confirmed  $z > 2$  Lyman break galaxies have been reported in the HDF (Steidel et al. 1996a; Lowenthal et al. 1997).

In this paper we construct the broadband optical and IR (i.e., rest-frame UV and optical) spec-

tral energy distributions (SEDs) of the 17 spectroscopically confirmed Hubble Deep Field Lyman break galaxies (§ 2). These observed SEDs are then fitted with dust-corrected spectral synthesis models described in § 3.1. These fits show that light from Lyman break galaxies is attenuated by significant amounts of dust (typically  $E(B - V) \approx 0.3$ ; § 3.2) and is dominated by very young ( $\lesssim 0.2Gyr$ ) stellar populations (§ 3.3). Furthermore, Lyman break objects have high rates of star formation (typically  $\sim 60h_{100}^{-2}M_{\odot}yr^{-1}$  for  $q_0 = 0.5$ ; § 3.4), and quite low stellar masses (typically,  $\sim 10^9h_{100}^{-2}M_{\odot}$ ; § 3.5). Since internal reddening in Lyman break galaxies appears to be significant, in § 4.1 we calculate its effects on the recently-published estimates of  $z > 2$  star formation and metal ejection rates. In § 4.2 we speculate on the nature of Lyman break galaxies in view of the high star formation rates and young ages of stellar populations which we found earlier. Our results are summarized in § 5.

## 2. DATA

We study the broadband spectral energy distributions for the 17 spectroscopically confirmed  $z > 2$  HDF objects reported by Steidel et al. (1996b; 6 objects<sup>3</sup>, some with revised redshifts<sup>4</sup>) and by Lowenthal et al. (1997; 11 objects). We measured broadband fluxes using both optical (Williams et al. 1996) and infrared (Dickinson et al. 1997) data. Specifically, in the optical we used the publicly-available Version 2,  $4 \times 4$  binned, HST images of the HDF; in the IR we employed the, also publicly available, Version 1 Kitt Peak 4m IRIM observations. The use of the IR data is crucial, as at  $z \sim 3$  the optical data alone give coverage only bluewards of rest-2000 Å, while the IR extends this to rest-5500 Å, thereby spanning the age-sensitive Balmer break. Altogether, the available photometry spans 3000 – 22000 Å (or 750 – 5500 Å at  $z = 3$ ) in 7 bandpasses ( $U_{300}$ ,  $B_{450}$ ,  $V_{606}$ ,  $I_{814}$ ,  $J$ ,  $H$ ,  $K_s$ )<sup>5</sup>, although, as will be explained later, we do not include the  $U_{300}$  and  $B_{450}$  data in our fits.

We smoothed the HST images to match the poorer, ground-based point spread function (PSF) of the IR images. We then performed photometry using the PPP faint galaxy photometry package

---

<sup>3</sup>Steidel et al. report five  $z > 2$  redshifts. Since, morphologically, C4-06 appears to have two distinct components, we have treated it as two objects at a common redshift.

<sup>4</sup>The redshift of the Steidel et al. (1996b) object C5-02 has been revised from  $z = 2.845$  to  $z = 2.008$  (Steidel, private communication). The reported redshift of C3-02 may also be erroneous: The observed broadband SED of C3-02 (Figure 1) exhibits a break between the  $I_{814}$  and  $J$  filters and not, as would have been expected of the Balmer break in a  $z = 2.775$  object, redward of  $J$ . We note that the absorption lines of C IV 1550, Fe II 1608, and Al II 1670 could be misidentified as Ly  $\alpha$  1216, Si II 1260, and O I 1303. In this case the redshift of C3-02 would be  $z = 1.95$ , which is consistent with the photometric redshift  $z_{phot} = 2.1$  of Sawicki et al. (1997) and with the placement of the Balmer break between the  $I_{814}$  and  $J$  filters. While adopting the revised redshift for C5-02, we retain the published value for C3-02. We tested the effects of this possible redshift misidentification on our analysis and found them to be small.

<sup>5</sup> $U_{300}$ ,  $B_{450}$ ,  $V_{606}$ , and  $I_{814}$  are used to denote the HST filters  $F300W$ ,  $F450W$ ,  $F606W$ , and  $F814W$ .

(Yee 1991). Colors were measured in “color apertures”: for each object, a color aperture was chosen so as to maximize the S/N. Photometric calibration was based on the zeropoints provided in the STScI-HDF and KPNO-IRIM-HDF web pages (Ferguson 1996; Dickinson 1996), while conversion to AB magnitudes (for the IR data) was done using the  $F_\nu(0 \text{ mag})$  fluxes of Wemstaker (1981). The photometry results are presented in Table 1. The magnitudes listed are “total magnitudes” obtained by correcting the object’s magnitude within the color aperture by its growth curve in the  $V_{606}$  image. A typical total magnitude aperture is  $3.2''$ .

### 3. COMPARISON WITH SPECTRAL SYNTHESIS MODELS

#### 3.1. The Models

For the analysis of the stellar populations of Lyman break galaxies, we generated a set of model broadband SEDs constructed in the following way: We started with the Bruzual & Charlot (1996) multi-metallicity spectral synthesis models; specifically, we used the KL96 theoretical stellar spectra<sup>6</sup> with the Salpeter  $0.1 < \frac{m}{M_\odot} < 125$  IMF. These Bruzual & Charlot models were attenuated with Calzetti’s (1997; see also Calzetti et al. 1994) empirical reddening recipe for star-forming galaxies<sup>7</sup>, covering a range of  $E(B - V)$  values. The reddened SEDs were appropriately redshifted and then convolved with the instrumental transmission curves (in the case of the HST data) or filter transmission curves (for the Kitt Peak IR observations) producing a suite of model colors. For each object this suite of model colors contains two possible star formation histories (instantaneous burst and constant star formation), 221 ages (0–20 Gyr), three different metallicities ( $0.02Z_\odot$ ,  $0.2Z_\odot$ , and  $1.0Z_\odot$ ), and a range of reddening ( $E(B - V) = 0.0$  to  $0.5$  in steps of  $0.02$ ).

Why were these particular ingredients chosen for the models? *Initial mass function:* The initial mass function, at least in low-redshift starbursts, appears to be independent of environment and is consistent with the Salpeter IMF with a high ( $\sim 100M_\odot$ ) upper mass cutoff (Stasińska & Leitherer 1996; see also Massey et al. 1995). We have thus chosen to use the Salpeter  $0.1 < \frac{m}{M_\odot} < 125$  IMF available in the Bruzual & Charlot (1996) library. *Reddening curve:* Since, by virtue of their color selection criteria (Steidel et al. 1996b; Lowenthal et al. 1997), the 17 spectroscopically confirmed HDF Lyman break objects are star-forming, the use of the Calzetti (1997) reddening curve for

---

<sup>6</sup>In general, substantial differences still exist between composite SEDs based on theoretical and empirical stellar spectra. We have, however, tested our dust and age results with Bruzual & Charlot solar-metallicity empirical models and found that the differences were small for our purposes.

<sup>7</sup>Calzetti (1997) gives:

$$F_{obs}(\lambda) = F_0(\lambda)10^{-0.4E(B-V)k(\lambda)},$$

where

$$k(\lambda) = \begin{cases} [(1.86 - 0.48/\lambda)/\lambda - 0.1]/\lambda + 1.73 & \text{for } 0.63\mu\text{m} \leq \lambda \leq 1.0\mu\text{m} \\ 2.656(-2.156 + 1.509/\lambda - 0.198/\lambda^2 + 0.011/\lambda^3) + 4.88 & \text{for } 0.12\mu\text{m} \leq \lambda < 0.63\mu\text{m} \end{cases}$$

star-forming regions is appropriate. Unlike the commonly-used LMC and SMC reddening curves (Fitzpatrick 1986; Bouchet et al. 1985) which are derived for stars alone, the Calzetti curve holds for star-forming *regions*; it thus automatically includes such effects as back-scattering and geometrical distribution of dust and is therefore much more appropriate for correcting the effects of dust on the photometry of star-forming galaxies (Gordon, Calzetti, & Witt 1997). Using the LMC reddening law would produce extinction values 2.5–3 times lower than that which we find (§ 4.1) with the more appropriate Calzetti extinction curve. *Metallicity*: Damped Ly- $\alpha$  systems at  $z = 2-3$  have metallicities  $Z \lesssim 0.1Z_{\odot}$  (Pettini et al. 1994; Lu et al. 1996; Pettini et al. 1997a); thus  $0.2Z_{\odot}$  or  $0.02Z_{\odot}$  are reasonable values to expect for the metallicity of Lyman break galaxies, while  $1.0Z_{\odot}$  provides a useful check in case the metallicity of Lyman break objects were significantly higher than that of damped Ly- $\alpha$  clouds. *Ages*: At  $z \approx 3$  the Universe is only 1 – 2 Gyr old and no object within it can be older than that; we have, however, allowed for model ages of up to 20 Gyr as a consistency check of the fits. *Star formation history*: In reality, the most likely star-formation scenario is that of a burst in which the star formation rate (SFR) declines with time. The two star formation histories used (instantaneous burst and constant SFR) thus provide the bracketing cases of the likely star formation histories of these objects. Dust contents and ages of stellar populations obtained from these two extremes will then bracket the actual values of age and reddening.

For high-redshift objects, the neutral hydrogen contained in Ly- $\alpha$  clouds along the line of sight provides an extra source of opacity in the UV (e.g., Madau 1995). The amount of extinction provided by this mechanism is stochastic and depends on the numbers, redshift distribution, and column densities of the Ly- $\alpha$  clouds along the line of sight to the target galaxy. The galaxy’s UV flux is affected blueward of rest-1216 Å and is almost completely extinguished below rest-912 Å. Whereas this effect is of great usefulness in identifying high- $z$  galaxies, its stochastic nature introduces uncertainties below  $\sim 1200$  Å in the SED models for individual galaxies. These stochastic uncertainties, combined with the fact that the dust reddening curve is not well known below 1200 Å, led us to decide not to fit the two bluest filters ( $U_{300}$  and  $B_{450}$ ). Thus all the fits presented in this paper have been done using the 5 reddest filters ( $V_{606}$ ,  $I_{814}$ ,  $J$ ,  $H$ , and  $K_s$ ).

Metallicity ( $Z = 0.02Z_{\odot}$ ,  $0.2Z_{\odot}$ , and  $1.0Z_{\odot}$ ) and star formation history (instantaneous burst and constant SFR) were fixed, giving six scenarios. In each of these six scenarios, age since the onset of star formation and amount of dust were free parameters. The models and the data were compared by means of  $\chi^2$  minimization. As an illustration, Figure 1 shows the fits thus obtained with the  $0.2Z_{\odot}$  continuous-SFR models. Instantaneous burst models, as well as those for  $Z = 0.02Z_{\odot}$  and  $1.0Z_{\odot}$ , produced fits of similar quality. Note that the two bluest filters, although not used to produce the fit, match the best-fitting model SEDs quite well.

Because reddening increases towards shorter wavelengths, the part of the SED which contains information about dust attenuation is the rest-frame UV. Dust attenuation can, however, be mimicked by aging of the stellar population: as the population ages, massive stars die out and the UV flux decreases. For example, below rest-3000Å a zero-age SED with  $E(B - V) = 0.3$  looks very much like a 100 Myr, constant SFR, dust-free one. The availability of IR data allows the lifting

of this degeneracy between age and reddening: at  $z > 2$ , IR data are probing the rest-optical part of the SED and consequently measure the age by means of the size of the Balmer break and, to a lesser degree, the slope of the continuum redward of rest-4000Å. Metallicity effects could pose a problem because of the age-metallicity degeneracy (e.g., Worthey 1994), but we have monitored their effects by performing fits with models of different metallicity ( $0.02Z_{\odot}$ ,  $0.2Z_{\odot}$ , and  $1.0Z_{\odot}$ ). As will be seen later, no overwhelming metallicity effects have been found.

With increasing redshift, the rest wavelengths probed by each filter move more and more blueward (by  $z \approx 3$ , the  $H$  filter is centered at 4000Å) and consequently less and less information is available about the age-sensitive rest-optical part of the SED. Thus, past  $z = 3$ , only one filter ( $K_s$ ) is redward of the 4000Å break. Because of this loss of age-sensitive information at higher redshifts, we have chosen to split the sample at  $z = 3$ . We consider fits for the 11 objects at  $z < 3$  to be much more reliable than those for the six at  $z > 3$ . The results and discussion presented below are mainly based on the 11  $z < 3$  galaxies; we will, however, retain the six  $z > 3$  objects for completeness and as a consistency check.

### 3.2. Dust Content

For each object the models described above fit simultaneously the dust content and the age of the dominant stellar population. The age and  $E(B - V)$  parameters of the best-fitting  $0.2Z_{\odot}$  models are plotted in Figure 2, with error bars corresponding to 90% confidence limits. The Figure illustrates that the Lyman break objects are best fitted by models which require non-zero amounts of dust. The median values for both the instantaneous burst and constant SFR  $0.2Z_{\odot}$  scenarios are  $E(B - V) = 0.28$ , producing a factor of 16 attenuation at 1600Å. This attenuation value is in agreement with the result derived from the UV spectral indices by Meurer et al. (1997) (see also Calzetti 1997). Note, however, that Meurer et al. had to assume (correctly, as we shall see in § 3.3) that the  $z > 2$  galaxies are no older than 0.3 Gyr.

Just as in the  $0.2Z_{\odot}$  case, the  $0.02Z_{\odot}$  and  $1.0Z_{\odot}$  models require significant amounts of dust. The results are summarized in Figure 3 which shows the distribution of  $E(B - V)$  values for the six different scenarios. Dust is required for the vast majority of galaxies in all of the six scenarios. For sub-solar metallicities ( $0.02Z_{\odot}$  and  $0.2Z_{\odot}$ ) typical values are  $E(B - V) \approx 0.3$  and somewhat lower ( $E(B - V) = 0.15 - 0.2$ ) for the unlikely case of solar metallicity.

Can dust-free models be securely ruled out? The error bars in Figure 2 are 90% confidence limits; hence, at 90% confidence, non-zero amounts of dust are unavoidable in all but one or two of the 11  $z < 3$  objects. The presence of dust is further illustrated in Figure 4, where, for three objects, the best possible dust-free models are compared with those in which dust is allowed. More qualitatively, the median reduced  $\chi^2$  are 1.34 and 1.68 for the instantaneous burst and constant SFR  $0.2Z_{\odot}$  fits with dust; the corresponding dust-free values are 5.04 and 10.1. Models with dust give much better fits than those without it. Therefore we conclude that dust is present in Lyman break

galaxies. A similar conclusion was reached by Ellingson et al. (1996) for the  $z = 2.72$  galaxy cB58, which has relatively high-precision IR photometry.

The high reddening values obtained here from broadband photometry of Lyman break galaxies are in contrast to the negligible extinctions inferred from chemical abundances in damped Ly $\alpha$  systems (Lu et al. 1996; Pettini et al. 1997a). However, while quasar sightlines probe essentially random regions of damped Ly $\alpha$  galaxies, broadband photometry targets regions of star formation. Thus, if the star-forming regions have substantially different dust-to-gas ratios than “random” parts of high-redshift galaxies, then the discrepancy between the damped Ly $\alpha$  spectroscopic and our photometric results may simply reflect the differences in the environments that the two methods probe.

Star formation rates have been derived from the fluxes of either H $\alpha$  or H $\beta$  for the small number of high-redshift objects for which these fluxes have been measured (Bechtold et al. 1997; Pettini et al. 1997b). In these objects, line-based SFR measurements are generally lower than the dust-corrected star-formation rates derived from UV fluxes. This apparent discrepancy can, however, be caused by a number of effects other than discrepant dust measurements; these effects include leakage of Lyman-limit photons from H II regions, absorption of Lyman-limit photons by dust, and a non-standard IMF (see Bechtold et al. 1997 and references therein). These effects may affect the reliability of SFR measurements based on emission lines. Ultimately, *concurrent* measurements of H $\alpha$ /H $\beta$  ratios will provide a robust and independent estimate of the dust content in Lyman break galaxies.

Based on our analysis, the presence of dust in Lyman break galaxies seems unavoidable with  $E(B - V) \approx 0.3$  being typical. As will be discussed in § 4.1, these amounts of dust are large enough to significantly affect estimates of star formation and metal ejection rates at high redshift.

### 3.3. Ages of Stellar Populations

For each galaxy, we shall date the age of the galaxy’s dominant stellar population. It must be emphasized that the age of the dominant stellar population does not mean the age of the galaxy itself, but rather corresponds to the time since the onset of the most recent major episode of star formation. Note that the instantaneous burst and constant SFR models are the limiting-case scenarios, while a galaxy’s star formation history probably lies somewhere between these two extremes. Thus, the instantaneous burst model provides the lower bound, while the constant SFR model gives the upper bound on the likely age of the galaxy’s current episode of star formation.

Figure 2 presents the parameters of the best-fitting  $0.2Z_{\odot}$  models, while Figure 5 shows the distribution of galaxy ages for all six combinations of metallicity and star formation history. As these Figures illustrate, in the constant SFR scenario the vast majority of  $z < 3$  objects, for which spectral coverage is sufficient in the red, are best fit with models for which the ages of dominant stellar populations are less than 0.2 Gyr. In the instantaneous burst scenario, the ages

of virtually all the objects, including the six with  $z > 3$ , are less than 0.1 Gyr. The median ages for the  $z < 3$  objects are 36 Myr and 10 Myr in the  $0.2Z_{\odot}$  constant SFR and instantaneous burst scenarios, respectively. Although objects at  $z > 3$  have insufficient IR coverage to constrain ages reliably, their fits are also consistent with very young stellar populations; for the instantaneous burst scenarios these ages are as young as for the  $z < 3$  objects.

How confidently can we rule out older ages of stellar populations? The error bars in Figure 2 are 90% confidence limits. If we consider the constant SFR model (which is more favorable for long ages), we see that of the  $z < 3$  objects all but one must have ages  $< 1$  Gyr at the 90% confidence level. A further illustration of the necessity of young ages is given in Figure 6: the (forced) 1 Gyr-old models produce poorer fits than the unforced younger models. More qualitatively, whereas the median reduced  $\chi^2$  are 1.34 and 1.68 for the  $0.2Z_{\odot}$  instantaneous burst and constant SFR models with free age, the corresponding values for the forced 1Gyr fits are 355.2 and 6.67, respectively. We therefore conclude that the  $z > 2$  Lyman break galaxies are dominated by very young stellar populations.

A possible concern is that the IMF employed to generate the models (i.e., the Salpeter  $0.1 < \frac{m}{M_{\odot}} < 125$  IMF) may not reflect the true IMF in the Lyman break galaxies. In particular, the determination of the age of the stellar population is primarily sensitive to the size of the Balmer break, which grows as the population ages. Since low-mass stars are responsible for the Balmer break, an IMF deficient in low-mass stars would produce a Balmer break that is smaller than expected for a given age, thereby mimicking the signature of a younger stellar population. Consequently, for an IMF deficient in low-mass star, our fits would underestimate the ages of stellar populations. The multi-metallicity SEDs of Bruzual & Charlot (1996) are available only for the  $0.1 < \frac{m}{M_{\odot}} < 125$  IMF. Hence, to estimate the impact of an IMF with a high lower-mass cutoff, we have compared the predicted colors of Bruzual & Charlot (1993) solar metallicity models with different IMF mass ranges. Specifically, we have compared the  $0.1 < \frac{m}{M_{\odot}} < 125$  and  $2.5 < \frac{m}{M_{\odot}} < 125$  Salpeter IMFs. The comparison reveals that, for the young ages in question and *if* the IMF is deficient in low-mass stars, the age of the star-forming population can be underestimated by a factor of  $\sim 5$  in the instantaneous burst scenarios; in the constant SFR models the underestimate is only at the 10% level. These effects would then increase the median age in either scenario to no more than  $\sim 50$  Myr. IMF effects are thus unlikely to affect our conclusion that the Lyman break objects have very young stellar populations.

Figure 7 shows, as a function of redshift, ages of stellar populations obtained with the  $0.2Z_{\odot}$  SEDs. The age of the  $q_0 = 0.5$ ,  $t_0 = 12.5$  Gyr Universe and the age of an object which formed at  $z_f = 4.5$  are shown for comparison. Lyman break galaxies are, by and large, dominated by very young stellar populations. The absence of older (age  $> 0.2$  Gyr) objects, particularly at the lower end of the redshift range covered, is remarkable. Possible reasons for this absence will be discussed in § 4.2.



### 3.4. Star Formation Rates

To estimate the star formation rates in Lyman break galaxies, we use the constant SFR fits. For each of the observed objects, we obtain the SFR by comparing the normalization of the fit to that of a  $1M_{\odot}yr^{-1}$  model of identical age and reddening. For the  $z < 3$  objects,  $0.2Z_{\odot}$  constant SFR models, and  $q_0 = 0.5$ , the median SFR is  $59h_{100}^{-2}M_{\odot}yr^{-1}$  ( $167h_{100}^{-2}M_{\odot}yr^{-1}$  for  $q_0 = 0.05$ ). The distribution of star formation rates in our sample is shown in Figure 8.

As a check on the star formation rates derived above from SED fitting, we can use the predicted rest-frame 1500 Å flux of a 9 Myr old,  $10^6M_{\odot}$  galaxy with a  $100 < \frac{m}{M_{\odot}} < 1$  Salpeter IMF (Leither et al. 1995). Comparing the dust-corrected, observed fluxes of the HDF Lyman break objects against the fiducial flux of Leitherer et al. gives a median SFR of  $63h_{100}^{-2}M_{\odot}yr^{-1}$  ( $q_0 = 0.5$ ), thereby confirming the SFR value obtained earlier from SED fitting.

For illustrative purposes, we have also computed the SFRs under the assumption that the Lyman break objects are dust-free. The resulting median star formation rate is  $2h_{100}^{-2}M_{\odot}yr^{-1}$  for  $q_0 = 0.5$  ( $6h_{100}^{-2}M_{\odot}yr^{-1}$  for  $q_0 = 0.05$ ), in agreement with the dust-free SFR estimates given by Steidel et al. (1996a) and Lowenthal et al. (1996). However, since models which include dust produce much better fits, we prefer the  $\sim 60h_{100}^{-2}M_{\odot}yr^{-1}$  ( $\sim 170h_{100}^{-2}M_{\odot}yr^{-1}$  for  $q_0 = 0.05$ ) dust-corrected rates of star formation.

### 3.5. Stellar Masses

To estimate the stellar masses produced in Lyman break galaxies, we can use the results of either the instantaneous burst fits or the constant SFR fits. For the instantaneous burst fits, we compute the stellar mass formed in each of the observed objects by comparing the normalization of the fit to that of a  $1M_{\odot}$  model of identical age and reddening. For the  $z < 3$  objects,  $0.2Z_{\odot}$  instantaneous burst models, and  $q_0 = 0.5(0.05)$ , the median mass in stars is  $1(2) \times 10^9h_{100}^{-2}M_{\odot}$ , or about  $\frac{1}{30}$  ( $\frac{1}{15}$ ) the stellar mass of a present-day  $L^*$  galaxy ( $3 \times 10^{10}h_{100}^{-1}M_{\odot}$ ; Cowie et al. 1995).

Under the constant SFR assumption, the typical duration of a starforming episode is  $2 \times$  the median observed age. Using the ages and SFRs from the constant SFR fits, we get the median stellar mass to be  $2(4) \times 10^9h_{100}^{-2}M_{\odot}$  for  $q_0 = 0.5(0.05)$  — in agreement with the value derived from instantaneous burst fits. As was the case for star formation rates, comparing dust-corrected UV fluxes to Leitherer et al. models confirms the above masses. The distributions of stellar masses for both the instantaneous burst and constant SFR models are shown in Figure 9(b–c). In both scenarios, the stellar masses of Lyman break objects are generally smaller than the stellar mass of a present-day  $L^*$  galaxy. Stellar masses appear to be relatively insensitive to the details of star formation history.

As an illustration, the above analysis can also be applied to the fits obtained with dust-free models. For  $q_0 = 0.5(0.05)$ , under the instantaneous burst assumption, the resulting median stellar

mass is  $1(4) \times 10^9 h_{100}^{-2} M_{\odot}$ . Using the ages and star formation rates of the constant-SFR fits gives the median stellar mass of  $6(16) \times 10^9 h_{100}^{-2} M_{\odot}$ . These values, obtained from dust-free model fits, are surprisingly similar to the stellar masses derived from models which account for dust. In the instantaneous burst case, this agreement arises because the dust-free fits give older ages, which necessitates larger stellar masses to account for the observed fluxes. In the constant SFR case the agreement occurs because the lower star formation rate of the dust-free models are offset by their older ages.

The relative insensitivity of the total stellar mass formed to the assumed star formation history and dust content of the galaxy allows us to obtain a robust result for the typical mass produced by a star formation episode in a Lyman break galaxy. Averaging the median masses calculated from the dust-corrected instantaneous burst and constant SFR fits, we have that the median stellar mass produced in an episode of star formation in an HDF Lyman break galaxy is  $\sim 1.5(3) \times 10^9 h_{100}^{-2} M_{\odot}$  for  $q_0 = 0.5(0.05)$ . This median stellar mass is within the  $10^{10} M_{\odot}$  upper limits on the *gravitational* masses of HDF Lyman break galaxies which were obtained by Lowenthal et al. (1997) on the basis of Ly $\alpha$  emission line widths and is equivalent to  $\sim \frac{1}{20}$  ( $\frac{1}{10}$ ) the stellar mass of a present-day  $L^*$  galaxy.

## 4. IMPLICATIONS

### 4.1. Dust Corrections

Intervening dust has the effect of absorbing UV photons, thereby suppressing the observed UV flux. If, as the SED fits discussed in § 3.2 indicate,  $z > 2$  objects have substantial amounts of internal reddening, recent measurements of the rates of star formation (Steidel et al. 1996a; Madau et al. 1996; Lowenthal et al. 1997) and metal ejection (Madau et al. 1996; Sawicki et al. 1997) need to be revised.

Steidel et al. (1996a) have used rest-1500Å fluxes to estimate the average star formation rate of their Lyman break galaxy sample to be  $2h_{100}^{-2} M_{\odot} yr^{-1}$  for  $q_0 = 0.5$  (and  $6h_{100}^{-2} M_{\odot} yr^{-1}$  for  $q_0 = 0.05$ ). If we assume that their objects suffer from the same amount of reddening as is typical for the Lyman break objects in the Hubble Deep Field ( $E(B - V) \approx 0.28$ ), then their SFR estimates need to be adjusted upward to  $38h_{100}^{-2} M_{\odot} yr^{-1}$  for  $q_0 = 0.5$  (and to  $111h_{100}^{-2} M_{\odot} yr^{-1}$  for  $q_0 = 0.05$ ).

On the basis of 1500Å fluxes, Lowenthal et al. (1997) made estimates of star formation rates both in individual  $z \approx 3$  HDF objects and in the volume-averaged population. Reddening correction would bring the Lowenthal et al. range of star formation rates to  $13 - 35h_{100}^{-2} M_{\odot} yr^{-1}$  for  $q_0 = 0.5$  ( $31 - 111h_{100}^{-2} M_{\odot} yr^{-1}$  for  $q_0 = 0.05$ ). The volume-averaged star formation rates given by Lowenthal et al. need likewise be adjusted upwards by a factor of  $\sim 18$ .

Madau et al. (1996) studied a sample of U- and B-band dropouts in the Hubble Deep Field. They used the comoving UV (1620 Å at  $\langle z \rangle = 2.75$  and 1630 Å at  $\langle z \rangle = 4.0$ ) luminosity densities

to estimate the volume-averaged rates of metal ejection and star formation. If we apply the typical  $E(B - V) = 0.28$  extinction found to occur in  $z > 2$  galaxies, the Madau et al. estimates of both the star formation and metal ejection rates need to be revised upward by a factor of 16. This value is consistent with the factor of 15 derived by Meurer et al. (1997) on the basis of optical data alone and with the (as we have seen, correct) assumption of young ages. Note, however, that the Madau et al. (1996) estimates do not include incompleteness corrections, so they remain lower limits even after having been corrected for dust.

As part of their photometric redshift study of the Hubble Deep Field, Sawicki et al. (1997) have calculated the expected metal density of the Universe as a function of redshift. To do so, they have used rest-3000Å luminosity densities. Applying  $E(B - V) = 0.28$  of extinction yields a factor of 7 increase in flux at 3000Å, requiring a factor of 7 increase in the  $2 \lesssim z \lesssim 3.5$  metallicity of the Universe shown in Fig. 10. of Sawicki et al.

In summary, the values of star formation and metal ejection rates presented in the literature are underestimates, since they do not account for intrinsic reddening. Though the exact correction factors depend on the wavelength used for the original estimate, once correction for dust is made, both star formation and metal ejection rates go up by about an order of magnitude. Note that although the total mass of stars formed per object is similar for the dust-free and dust-included models (§ 3.5), the difference in the volume-averaged star formation and metal ejection rates of the Universe enters via the very different duty cycle of visibility which the Lyman break objects have in these two models.

#### 4.2. Ages and Star Formation Histories of Lyman Break Galaxies

For all but one of the  $z < 3$  HDF Lyman break galaxies, the ages of the dominant stellar populations are  $< 0.2$  Gyr. Since our redshift range ( $2 < z < 3.5$ ) spans a Gyr in time, the lack of a significant number of galaxies with old ( $> 0.2$  Gyr) stellar populations suggests that, in Lyman break galaxies, the duration of star formation is short rather than extended and continuous.

In the rest of this section we will speculate on some of the possible interpretations of this episodic star formation. Using simple calculations, we will show that under this single-burst scenario the number densities of Lyman break objects, in addition to their stellar masses, are consistent with Lyman break objects being progenitors of present-day  $L < L^*$  galaxies. They are unlikely to be the present-day  $L \geq L^*$  galaxies caught in the act of creation unless one invokes more complicated mechanisms such as mergers or recurrent bursts of star formation.

In the simplest scenario, akin to the low-mass starburst model of Lowenthal et al. (1997), each Lyman break galaxy undergoes a single episode of star formation. Since the stellar mass produced in a typical Lyman break galaxy is  $\sim 10^9 h_{100}^{-2} M_\odot$  (§ 3.5), such a burst would result in a low-mass object whose stellar mass is  $\sim \frac{1}{20}$  that of a present-day  $L^*$  galaxy. This typical mass is thus too low to account for the whole stellar mass of the bulge of a present-day  $L^*$  galaxy.

The young ages of their stellar populations, together with the fact that they will fade rapidly after star formation ends (by  $\sim 1$  magnitude in a mere 30 Myr), mean that only a small fraction of such short-burst galaxies are visible at any one time. The redshift range covered by the HDF Lyman break sample ( $2 < z < 3.5$ ), spans a time interval of  $\sim 0.8$  Gyr in a  $h_{100} = 0.7$ ,  $q_0 = 0.5$  universe ( $\sim 2.3$  Gyr for  $h_{100} = 0.7$ ,  $q_0 = 0.05$ ). The median age from the  $0.2Z_{\odot}$ , constant SFR fits is  $\sim 35$  Myr. Assuming that a typical star-forming burst lasts twice that time, and that it takes  $\sim 30$  Myr for the galaxy to fade  $\sim 1$  magnitude (and hence out of the spectroscopic sample), we estimate that a typical Lyman break galaxy stays in the sample for  $\sim 100$  Myr. Therefore, for every galaxy that is detected, there will be  $\sim 8$  ( $\sim 23$  for  $q_0 = 0.05$ ) objects which have faded beyond spectroscopic detectability. Hence, in the volume and redshift range sampled, there should be a total of  $\sim 136$  ( $\sim 391$ , for  $q_0 = 0.05$ ) visible *plus* faded objects which are undergoing, or have undergone, brief but intense bursts of star formation.

The comoving number density of this combined (both visible and faded) population is  $7 \times 10^{-2} h_{100}^3 \text{Mpc}^{-3}$  ( $4 \times 10^{-2} h_{100}^3 \text{Mpc}^{-3}$  for  $q_0 = 0.05$ ). In the  $K_s$ -band (which corresponds to  $\sim \text{rest-}V$ ), the HDF Lyman break galaxies span a range of  $\sim 2.5$  magnitudes. Locally, over a corresponding magnitude range, one expects to see  $\sim 2 \times 10^{-2} h_{100}^{-3} \text{Mpc}^{-3}$  galaxies with  $L \approx \frac{1}{20} L^*$  (Loveday et al. 1992; Lin et al. 1996). The number density of HDF Lyman break objects is thus similar to, or perhaps somewhat higher than, that of local  $\frac{1}{20} L^*$  galaxies. Thus, on the basis of their number densities and stellar masses, Lyman break objects are consistent with being progenitors of present-day sub- $L^*$  galaxies.

One could postulate that present-day  $L > L^*$  galaxies formed through bursts of star formation which are analogous to those which seem to be producing the above-mentioned low-mass objects, but which are more intense though less numerous than the bursts seen in the HDF. Based on the present-day luminosity function of Lin et al. (1996), and assuming that the 17 objects seen in the HDF are precursors of present-day sub- $L^*$  galaxies, one would expect the HDF to yield  $\sim 5$  Lyman break objects with stellar masses  $\geq 3 \times 10^{10} M_{\odot}$ , the expected stellar mass of an  $L^*$  galaxy. The fact that such massive stellar populations are absent (Figure 9) implies that most present-day massive galaxies did not form in single bursts of star formation at  $z > 2$ .

There are, however, alternative ways to assemble massive objects. One option is through galaxy-galaxy merging: the present-day merger rate is rather low but increases as  $(1+z)^{\sim 3-4}$ , at least to moderate redshift (e.g., Yee & Ellingson 1995; Patton et al. 1997). If this redshift trend continues to  $z \sim 3$ , then the merging of a dozen or so Lyman break objects can easily result in the spheroid of a present-day  $L^*$  galaxy.

Another possibility is akin to the ‘‘Christmas tree’’ model of Lowenthal et al. (1997; see also Colley et al. 1996). In this model, star formation is episodic but recurrent within each galaxy: star-forming episodes are separated by quiescent intervals during which the galaxy temporarily fades out of the sample. The underlying stellar population, resulting from previous star-forming bursts, would be too faded to be detectable in the presence of an ongoing burst (e.g., Ellingson et al. 1996).

Each of the recurrent star-forming bursts would then add, typically,  $\sim 10^9 h_{100}^{-2} M_\odot$  of new stars to the galaxy, gradually building up its stellar mass. A spheroid containing  $\sim 3 \times 10^{10} h_{100}^{-1} M_\odot$  worth of stars could be thus accumulated in a dozen or two such recurrent starburst episodes.

## 5. CONCLUSIONS

We have fitted the broadband spectral energy distributions of spectroscopically confirmed  $z > 2$  HDF Lyman break objects, using the multi-metallicity spectral synthesis models of Bruzual & Charlot (1996). In the fits we have included correction for internal dust extinction typical of local star-forming galaxies (Calzetti 1997). The fits also assume that the IMF at high redshift is not unlike that seen locally, although some leeway is allowed, particularly in the lower mass cutoff.

We find that Lyman break galaxies are dominated by very young stellar populations ( $< 0.2$  Gyr). The absence of objects with old stellar populations, particularly at lower redshifts ( $z \gtrsim 2$ ), implies that star formation in a typical Lyman break galaxy cannot go on continuously for a prolonged time. Instead, star formation must occur in bursts of short duration ( $t < 0.2$  Gyr).

A typical Lyman break galaxy is shrouded in enough dust to suppress its UV flux by a factor of  $\sim 16$  at  $1600\text{\AA}$ . Consequently, recent UV-based estimates of the rates of star formation and metal ejection at high redshift (Steidel et al. 1996a; Madau et al. 1996; Sawicki et al. 1997; Lowenthal et al. 1997) need to be adjusted upwards by a similar factor.

Star formation rates in Lyman break galaxies are high (median of  $59 h^{-2} M_\odot \text{yr}^{-1}$  for  $q_0 = 0.5$ ). These star formation rates typically produce  $10^9 h^{-2} M_\odot$  of stellar mass during the lifetime of a star-forming episode; this number is robust as it is relatively insensitive to the details of star formation history and dust content. This median stellar mass is equivalent to  $\frac{1}{15} - \frac{1}{20}$  the stellar mass contained in a present-day  $L^*$  galaxy. Objects with larger stellar masses may be built up through recurrent episodes of star formation, or can be assembled through mergers.

A stellar population will fade rapidly after the end of a brief episode of star formation ( $\sim 1$  magnitude at rest- $2000\text{\AA}$  in the first 30 Myr). Because star formation in Lyman break galaxies is of brief duration, a substantial population of objects which have just recently faded out of the spectroscopic sample may exist at high redshift. We estimate that if a typical Lyman break galaxy stays in our sample for 0.1 Gyr, then there are 8–23 such faded galaxies for every visible one. The number density of the combined visible and faded population (a few  $\times 10^{-2} h_{100}^3 \text{mag}^{-1} \text{Mpc}^{-3}$ ) is comparable to the number density of present-day sub- $L^*$  ( $M_B \gtrsim -18$ ) galaxies.

On the basis of the evidence presented above, we conclude that Lyman break objects are likely direct progenitors of present-day **sub- $L^*$**  galaxies, or that they may form luminous galaxies through merging or by repeated episodes of star formation. They do *not* appear to be steadily star-forming direct progenitors of present-day massive galaxies.

We thank Gabriela Mallén-Ornelas for a very thorough reading of an earlier version of this paper. We also thank Huan Lin, Bob Abraham, Gerhardt Meurer, and the anonymous referee for discussions and comments. This work was financially supported by NSERC of Canada.

## REFERENCES

- Bechtold, J., Yee, H.K.C., Elton, R., & Ellingson, E. 1997, ApJ, 477, L29
- Bouchet, P., Lequeux, J., Maurice, E., Prévot, L., & Prévot-Burnichon, M. L. 1985, A&A, 149, 330
- Bruzual A., G., & Charlot, S. 1993, ApJ, 405, 538
- Bruzual A., G., & Charlot, S. 1996, in preparation
- Calzetti D., 1997, to appear in the Proceedings of the Conference “The Ultraviolet Universe at Low and High Redshift” preprint: astro-ph/9706121
- Calzetti, D., Kinney, A., & Storchi-Bergmann, T. 1994, ApJ, 429, 582
- Cohen, J. G., Cowie, L. L., Hogg, D. W., Songaila, A., Blandford, R., Hu, E. M., & Snopbell, P. 1996, ApJ, 471, L5
- Colley, W.N., Gnedin, O.Y., Ostriker, J.P., & Rhoads, J.E 1997, ApJ, 488, 579
- Connolly, A.J., Szalay, A.S., Dickinson, M., SubbaRao, M.U., & Brunner, R.J. 1997, ApJ, 486, L11
- Cowie, L.C., Hu, E.M., & Songaila, A. 1995, Nature, 377, 603
- Dickinson, M. 1996,  
[http://www.stsci.edu/ftp/science/hdf/clearinghouse/irim/irim\\_zeropts.html](http://www.stsci.edu/ftp/science/hdf/clearinghouse/irim/irim_zeropts.html)
- Dickinson, M., et al. 1997, in preparation.
- Ellingson, E., Yee, H.K.C., Bechtold, J., & Elston, R. 1996, ApJ, 466, L71
- Ferguson, H. 1996, <http://www.stsci.edu/ftp/observer/hdf/logs/zeropoints.txt>
- Fitzpatrick, E.L., 1986, AJ, 92, 1068
- Fomalont, E. B., Kellermann, K. I., Richards, E. A., Windhorst, R. A., & Partridge, B. P. 1997, ApJ, 475, L5
- Giavalisco, M., Steidel, C.C., & Macchetto, F.D. 1996, ApJ, 470, 189
- Gordon, K. D., Calzetti, D., & Witt, A. N. 1997, ApJ, 487, 626
- Hogg, D.W., Neugebauer, G., Armus, L., Matthews, K., Pahre, M.A., Soifer, B.T., & Weinberger, A.J. 1997, AJ, 113, 474
- Leitherer, C., Robert, C., & Heckman, T.M. 1995, ApJS, 99, 173
- Lin, H., Kirshner, R.P., Sackett, S.A., Landy, S.D., Oemler, A., Tucker, D., & Schechter, P.L. 1996, ApJ, 464, 60

- Loveday, J., Peterson, B.A., Efstathiou, G., & Maddox, S.J. 1992, ApJ, 390, 338
- Lowenthal, J.D., Koo, D.C., Guzmán, R., Gallego, J., Phillips, A.C., Vogt, N.P., Illingworth, G.D., & Gronwall, C. 1997, ApJ, 481, 673
- Lu, L., Sargent, W.L.W., Barlow, T.A., Churchill, C.W., & Vogt, S.S. 1996, ApJS, 107, 475
- Madau, P. 1995, ApJ, 441, 18
- Madau, P., Ferguson, H.C., Dickinson, M.E., Giavalisco, M., Steidel, C.C., & Fruchter, A. 1996, MNRAS, 283, 1388
- Massey, P., Lang, C.C., DeGioia-Eastwood, K., & Garmany, C.D. 1995, ApJ, 438, 188
- Meurer, G.R., Heckman, T.M., Lehnert, M.D., Leitherer, C., & Lowenthal, J. 1997, AJ, 114, 54
- Pascarelle, S. M., Windhorst, R. A., Keel, W. C., & Odewahn, S. C. 1996, Nature, 383, 45
- Patton, D.R., Pritchett, C.J., Yee, H.K.C., Ellingson, E., & Carlberg, R.G. 1997, ApJ, 475, 29
- Pettini, M., Smith, L.J., Hunstead, R.W., & King, D.L. 1994, ApJ, 426, 79
- Pettini, M., King, D.L., Smith, L.J., & Hunstead, R.W. 1997, ApJ, 478, 536
- Pettini, M., Steidel, C.C., Adelberger, K.L., Kellogg, M., Dickinson, M., & Giavalisco, M. 1997, to appear in *Origins*, ed. J.M. Shull, C.E. Woodward, and H. Thronson (ASP Conference Series); preprint: astro-ph/9708117
- Sawicki, M.J., Lin, H., & Yee, H.K.C. 1997, AJ, 113, 1
- Serjeant, S., Eaton, N., Oliver, S., Efstathiou, A., Goldschmidt, P., Mann, R.G., Mobasher, B., Rowan-Robinson, M., Sumner, T., Danese, L., Elbaz, D., Franceschini, A., Egami, E., Kontizas, M., Lawrence, A., McMahon, R., Norgaard-Nielsen, H.U., Perez-Fournon, I., & Gonzalez-Serrano, I. 1997, MNRAS, 289, 457
- Stasińska, G., & Leitherer, C. 1996, ApJS, 107, 472
- Steidel, C. C., Giavalisco, M., Pettini, M., Dickinson, M., & Adelberger, K.L. 1996a, ApJ, 462, L17
- Steidel, C. C., Giavalisco, M., Dickinson, M., & Adelberger, K.L. 1996b, AJ, 112, 352
- Steidel, C. C., Adelberger, K. L., Dickinson, M., Giavalisco, M., Pettini, M., Kellogg, M. 1997, ApJ, in press, preprint: astro-ph/9708125
- Wemstaker, W. 1981, A&A, 97, 329
- Williams, R. E., Blacker, B., Dickinson, M., Van Dyke Dixon, W., Ferguson, H. C., Fruchter, A. S., Giavalisco, M., Gilliland, R. L., Heyer, I., Katsanis, R., Levay, Z., Lucas, R. A., McElroy, D. B., Petro, L., Postman, M., Adorf, H.-M., & Hook, R. N. 1996, AJ, 112, 1335



Worthey, G. 1994, ApJS, 95, 107

Yee, H.K.C. 1991, PASP, 103, 396

Yee, H.K.C., & Ellingson, E. 1995 ApJ, 445, 37

Yee, H.K.C., Ellingson, E., Bechtold, J., Carlberg, R. G., & Cuillandre, J.-C. 1996 AJ, 111, 1783

Zepf, S.E., Moustakas, L.A., & Davis, M. 1997, ApJ, 474, L1

Table 1. Photometry

object	ref	$z$	$U_{300,AB}$	$B_{450,AB}$	$V_{606,AB}$	$I_{814,AB}$	$J_{AB}$	$H_{AB}$	$K_{s,AB}$
C2-05	S	2.008	25.72(06)	23.69(03)	23.47(03)	23.17(03)	22.79(05)	22.65(07)	22.23(05)
hd2_0725_1818	L	2.233	25.83(05)	24.39(03)	24.28(03)	24.19(03)	24.60(24)	23.73(17)	23.69(16)
hd2_2030_0287	L	2.267	26.46(06)	24.47(03)	24.35(03)	24.35(04)	24.16(15)	24.70(46)	24.22(30)
hd2_0624_0266	L	2.419	28.09(29)	25.14(03)	25.06(03)	25.09(04)	24.85(21)	24.55(35)	24.52(31)
C4-08	S	2.591	28.62(46)	24.57(03)	24.50(03)	24.31(03)	24.48(17)	24.50(32)	24.17(22)
C3-02	S	2.775	25.84(05)	24.64(03)	24.54(03)	24.50(03)	24.09(13)	> 24.27	24.33(25)
C4-06a	S <sup>a</sup>	2.803	27.67(22)	24.59(03)	23.47(03)	23.08(03)	22.97(07)	21.96(05)	21.82(04)
C4-06b	S <sup>a</sup>	2.803	27.33(12)	24.36(03)	24.03(03)	23.81(03)	23.46(08)	23.13(09)	22.87(08)
hd4_0367_0266	L	2.931	25.45(08)	24.77(04)	23.87(03)	23.54(03)	23.73(18)	22.54(11)	22.39(09)
hd4_2030_0851	L	2.980	> 29.37	25.39(04)	24.74(04)	24.45(04)	23.97(15)	23.97(27)	23.35(12)
hd2_0434_1377	L	2.991	29.74(26)	25.54(04)	24.66(03)	24.37(03)	24.64(19)	24.20(22)	24.18(20)
hd2_1410_0259	L	3.160	29.97(90)	25.38(04)	24.72(03)	24.66(04)	26.02(97)	24.58(56)	23.83(20)
hd2_1359_1816	L	3.181	> 29.56	25.82(04)	24.76(03)	24.35(03)	24.25(15)	23.73(15)	24.47(26)
C4-09	S	3.226	26.81(19)	25.01(03)	24.12(03)	23.87(03)	23.60(09)	24.01(24)	22.67(07)
hd3_0408_0684	L	3.233	> 29.26	25.88(04)	24.89(04)	24.40(04)	25.15(63)	24.98(78)	23.47(17)
hd2_0705_1366	L	3.368	27.55(21)	26.05(04)	25.04(03)	24.95(03)	26.08(74)	24.24(21)	24.47(23)
hd2_0698_1297	L	3.430	> 29.28	26.55(05)	25.19(03)	24.81(03)	25.28(32)	24.93(45)	23.62(12)

<sup>a</sup>Since object C4-06 has two very distinct components, we have treated it as two objects at the same redshift. C4-06a is the lower object in the C4-06 panel of Fig. 2 of Steidel et al. (1996b), while C4-06b is the upper object.

Note. — Upper limits ( $2\sigma$ ) are indicated with a “>”. Errors are indicated in parentheses: they are  $1\sigma$  uncertainties expressed as percentages of the *flux*.

References. — (S) Steidel et al. (1996b); (L) Lowenthal et al. (1997)

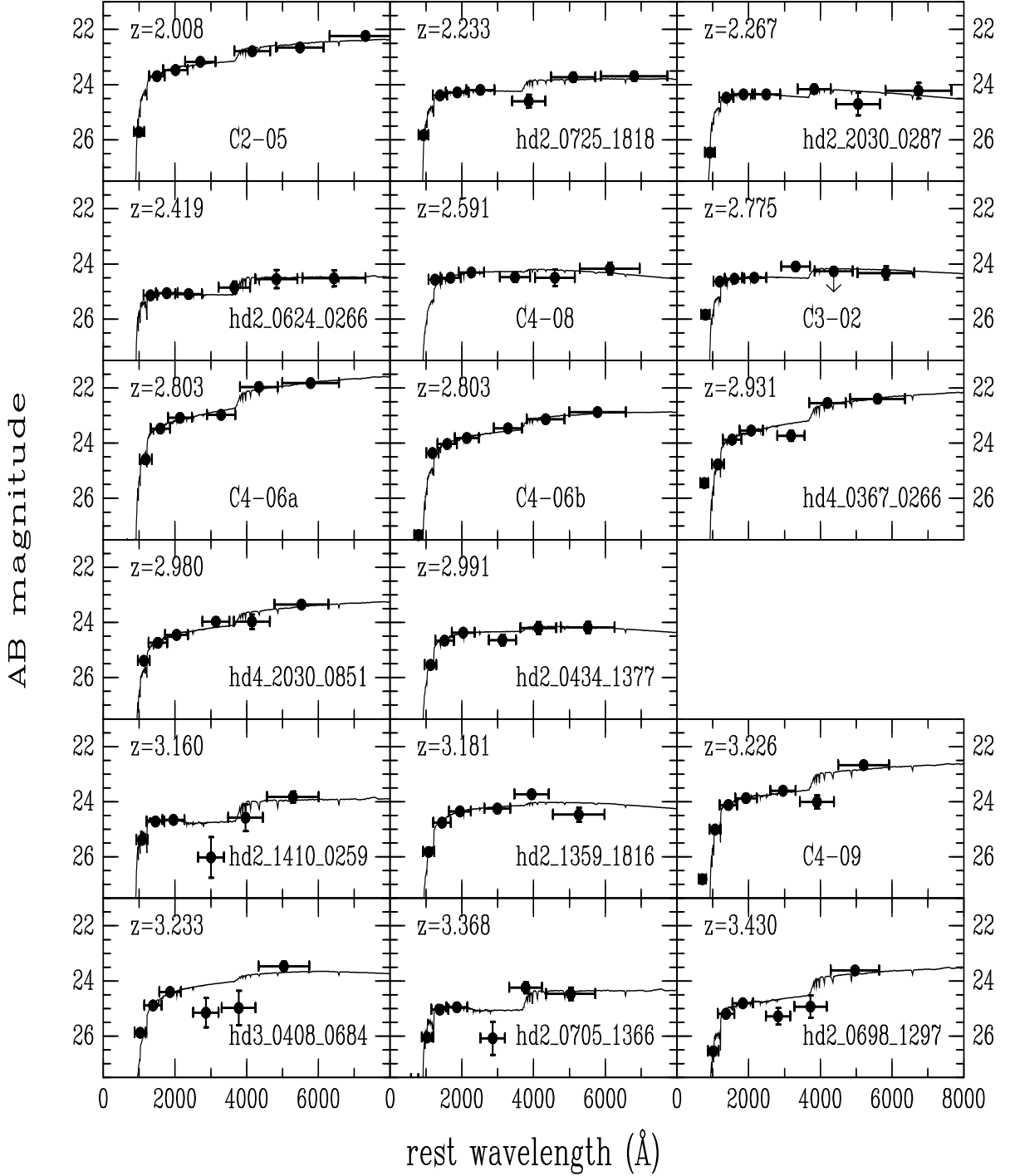


Fig. 1.— The best-fitting  $0.2Z_{\odot}$ , constant SFR models. Dust content and age are free parameters. Although their fluxes are plotted, the  $U_{300}$  and  $B_{450}$  data were not used in the fit (see text). The model SEDs shown include the high- $z$  Lyman suppression of the  $UV$  flux. The bottom two rows contain objects at  $z > 3$  — objects for which fit quality suffers from the fact that only one filter is present redward the Balmer break. Instantaneous burst and  $0.02Z_{\odot}$  and  $1.0Z_{\odot}$  models produced fits of similar quality as the ones shown here.

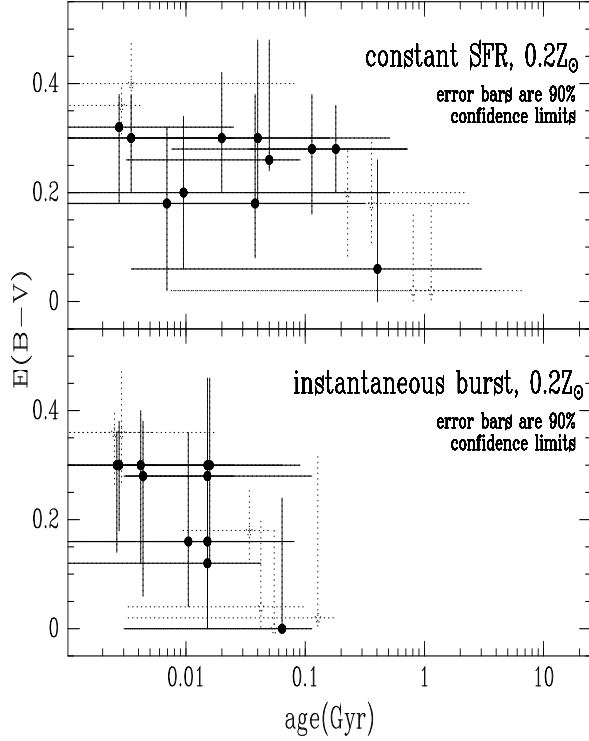


Fig. 2.— Reddening and age of the best-fit  $Z = 0.2Z_{\odot}$  models. The top panel shows the constant SFR fits and the bottom one is for the instantaneous burst model. Age is the time since the onset of star formation. Galaxies at  $z < 3$  are shown as solid symbols while those at  $z > 3$ , for which fit quality is poorer, use broken ones. Error bars come from  $\chi^2$  fitting and correspond to 90% confidence limits.  $Z = 0.02Z_{\odot}$  and  $1.0Z_{\odot}$  models produce similar results.

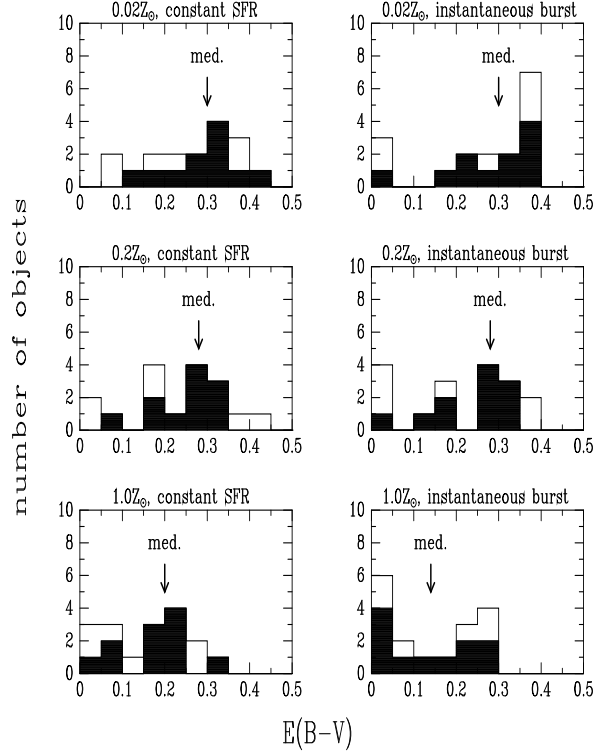


Fig. 3.— Intrinsic reddening for the 6 models of different metallicity and star formation history. The shaded histogram corresponds to those galaxies at  $z < 3$ , while the unshaded one is for all 17 objects (i.e., including the lower-quality  $z > 3$  fits). Arrows indicate the median values of  $E(B - V)$  for the  $z < 3$  galaxies. Substantial amounts of dust are present under all scenarios.

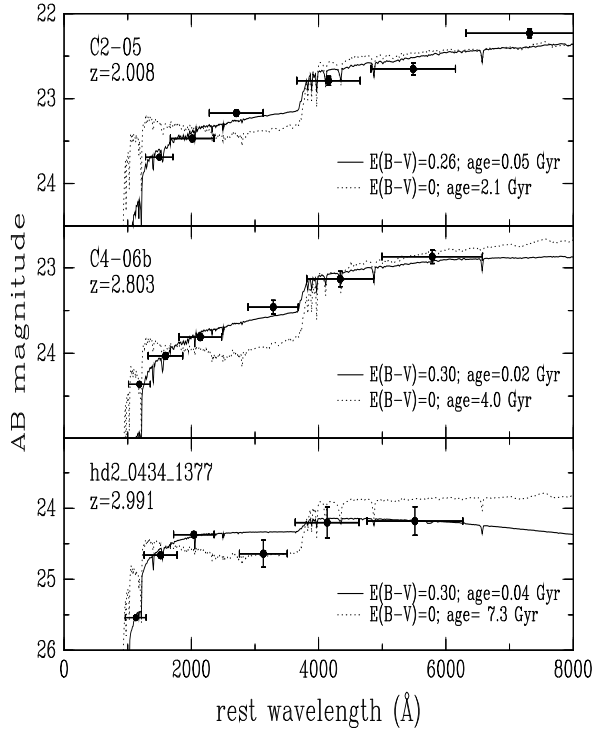


Fig. 4.— Examples of fits with and without dust for the  $Z = 0.2Z_{\odot}$  constant SFR models. The broken line shows the best-fit models for which age was allowed to vary freely, but  $E(B-V)$  was held at 0. The solid line shows the best-fit model (as in Figure 1) for which both age and dust were free parameters. Models with dust produce better fits than the dust-free ones.

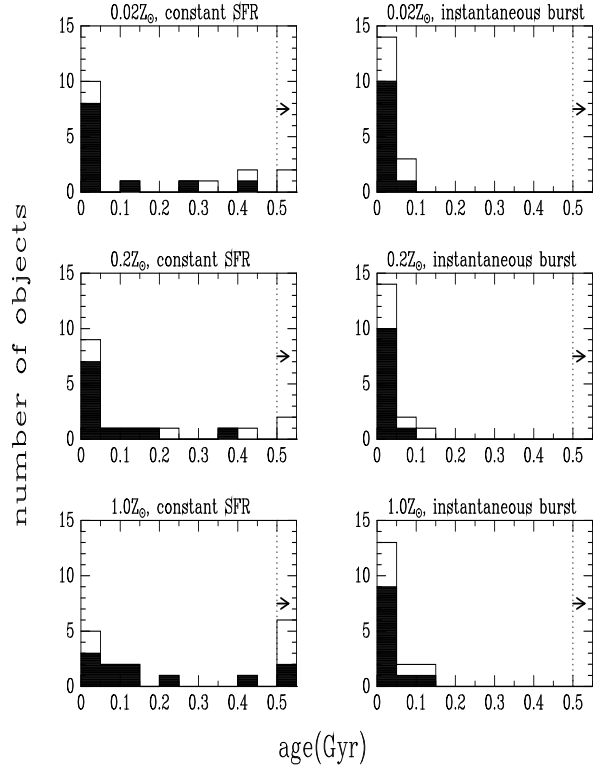


Fig. 5.— Ages since the onset of the current episodes of star formation. The shaded histogram corresponds to those galaxies at  $z < 3$ , while the unshaded one is for all 17 objects. Ages  $> 0.5$  Gyr are grouped together in the right-most bins (separated from the other bins by the dotted lines). Most Lyman break galaxies are dominated by very young stellar populations.

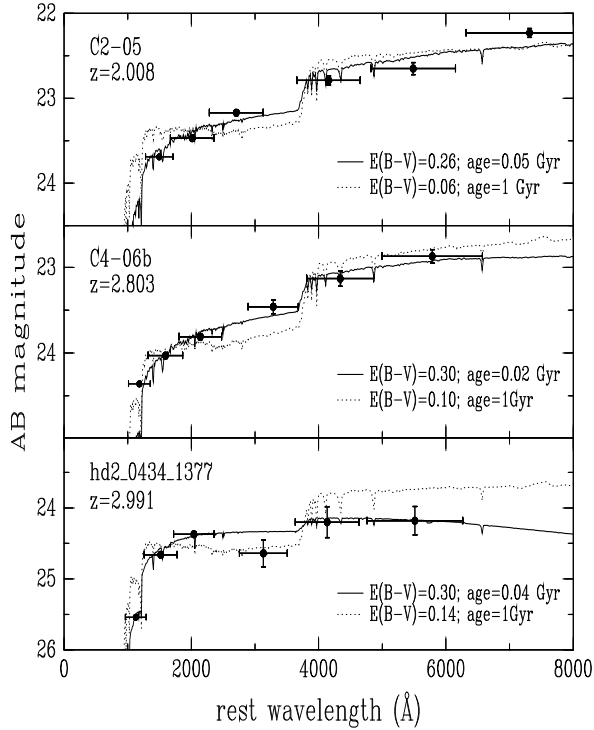


Fig. 6.— Examples of fits with and without forced age for the  $Z = 0.2Z_{\odot}$  constant SFR models. The broken lines are the fits for which age was fixed at 1 Gyr (while reddening was allowed to vary freely). The solid lines are the fits where, as in Figure 1, both age and reddening were free parameters. Instantaneous burst models of 1 Gyr age would produce an even stronger disagreement with the data, since in those models the UV-producing massive stars would not have continued to be replenished as in the constant SFR models.

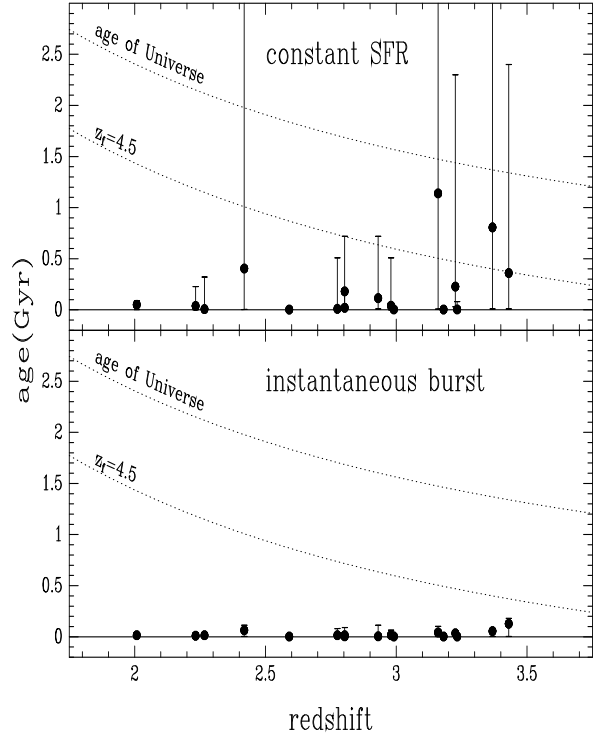


Fig. 7.— The ages of dominant stellar populations of Lyman break galaxies determined by fitting  $0.2Z_{\odot}$  model SEDs. Error bars correspond to 90% confidence limits. For comparison, the dotted lines show the age of the universe and the age of an object which formed at  $z_f = 4.5$ ; both are for a  $\Omega = 1$  universe with a present-day age fixed at  $t_0 = 12.5$  Gyr; note, however, that the stellar population ages do not depend on the value of  $H_0$ . Objects at  $z > 3$  suffer from poor coverage above  $\sim 4000$  Å and, consequently, have age estimates of lower quality. Models with  $Z = 0.02Z_{\odot}$  and  $1.0Z_{\odot}$  produce ages similar to these shown here. Stellar populations of the majority of  $z > 2$  HDF galaxies appear to have undergone recent ( $t < 0.2$  Gyr) episodes of star formation.

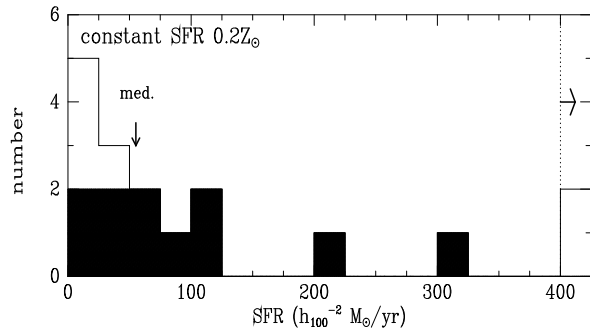


Fig. 8.— Distribution of star formation rates obtained from the  $0.2Z_{\odot}$  constant SFR fits. A  $q_0 = 0.5$  universe was assumed. The shaded histogram is for the eleven  $z < 3$  galaxies, and the unshaded one includes all 17 objects. The median value for the  $z < 3$  subset is indicated.

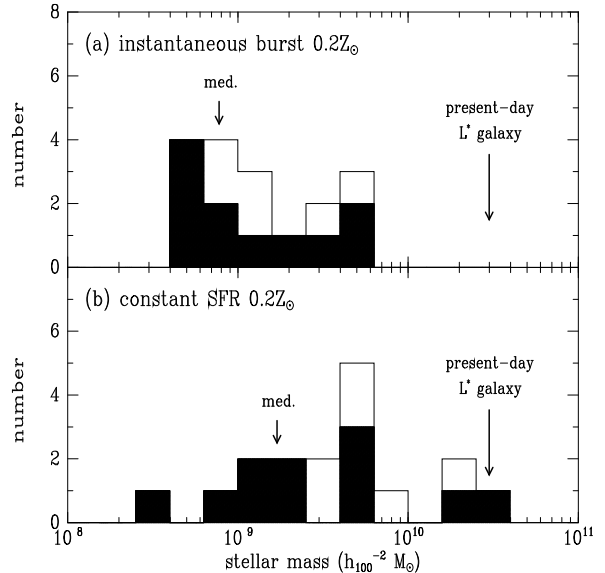


Fig. 9.— Stellar masses from the  $0.2Z_{\odot}$  fits. Shaded histograms are for  $z < 3$  galaxies, and the unshaded ones include all 17 objects. Arrows indicate median values for the  $z < 3$  subset. A  $q_0 = 0.5$  universe was assumed. Panel (a) shows the distribution of stellar masses obtained from the instantaneous burst fits. The stellar mass of a present-day  $L^*$  galaxy ( $3 \times 10^{10} h_{100}^{-1} M_{\odot}$ ; Cowie et al., 1995) is indicated for comparison. Panel (b) shows the distribution of stellar masses derived by multiplying the objects’ star formation rates and the ages of their stellar populations. Under both the instantaneous burst and constant SFR scenarios, stellar masses produced by the observed episodes of star formation are generally substantially less than the stellar mass of a present-day  $L^*$  galaxy.